Dynamics of colloidal particles in electrohydrodynamic convection of nematic liquid crystal

Kentaro Takahashi and Yasuyuki Kimura*

Department of Physics, School of Sciences, Kyushu University, 6-10-1 Hakozaki, Higashi-ku, Fukuoka 812-8581, Japan

(Received 17 March 2014; published 2 July 2014)

We have studied the dynamics of micrometer-sized colloidal particles in electrohydrodynamic convection of nematic liquid crystal. Above the onset voltage of electroconvection, the parallel array of convection rolls appears to be perpendicular to the nematic field at first. The particles are forced to rotate by convection flow and are trapped within a single roll in this voltage regime. A slow glide motion along the roll axis is also observed. The frequency of rotational motion and the glide velocity increase with the applied voltage. Under a much larger voltage where the roll axis temporally fluctuates, the particles occasionally hop to the neighbor rolls. In this voltage regime, the motion of the particles becomes two-dimensional. The motion perpendicular to the roll axis exhibits diffusion behavior at a long time period. The effective diffusion constant is 10^3–10^4 times larger than the molecular one. The observed behavior is compared with the result obtained by a simple stochastic model for the transport of the particles in convection. The enhancement of diffusion can be quantitatively described well by the rotation frequency in a roll, the width of the roll, and the hopping probability to the neighbor rolls.

DOI: 10.1103/PhysRevE.90.012502 PACS number(s): 83.80.Xz, 05.40.−a, 47.27.tb, 47.52.+j

I. INTRODUCTION

Particle dynamics in equilibrium viscous liquids is governed by the diffusion process driven by the thermal fluctuation of the surrounding liquids. The thermal diffusion constant is given by the Einstein relation and is determined by the viscosity of the fluids [1]. Recently, particle dynamics in nonequilibrium liquids such as a bacterial bath [2–5] and active actin gels [6] also have been studied much. The athermal motion in active fluids such as turbulence has been intensively studied as turbulent diffusion [7]. In stationary systems, the mean-square displacement (MSD) of a single particle is determined by the temporal velocity autocorrelation of the background fluids. This is different from the MSD due to the thermal Brownian motion, where the MSD is governed by the viscosity or thermal fluctuating force acting on the particles. This makes the diffusion constant of a particle in convective flows different from that of thermal diffusion. From such macroscopic viewpoints, the diffusion of the particles in convective flow has been investigated theoretically and experimentally [8–12].

In this study, we used the electrohydrodynamic (EHD) convection in nematic liquid crystal (NLC) as a typical active fluid. NLC is an anisotropic fluid with directional order, and anisotropic constituent molecules arrange uniaxially on average. Their direction is represented by a unit vector called a director. When an ac electric field is applied to an NLC with negative dielectric anisotropy in a planar cell where the constituent molecules are aligned parallel to the cell surfaces, a bifurcation process due to the EHD instability has been reported [13]. At first, the macroscopic convection roll whose axis is perpendicular to the direction of the initial director appears above a certain threshold voltage due to Carr-Helfrich instability. This pattern is called a Williams domain (WD) [14]. With increase of voltage, the WD becomes unstable, and the fluctuating WD (FWD) appears [15]. FWD is also referred to "defect turbulence" because the movement of defects and the fluctuation of the roll occur repeatedly and the roll pattern becomes more irregular. The defect turbulence has been studied as a typical spatiotemporal chaos, but it has not been fully understood. The control parameters which govern the appearing patterns are the magnitude and frequency of the applied electric field. Due to the experimental easiness of handling the system, the EHD of NLC has been intensively studied as one of the typical dispersive systems to elucidate nonlinear and nonequilibrium dynamics.

In the case of a homeotropic cell where the NLC molecules are aligned vertically to the cell surfaces, the continuous rotational symmetry of the director is spontaneously broken above a threshold voltage of Fréedericksz transition. The system bifurcates to the phase called soft mode turbulence (SMT) [16,17]. The SMT has two modes: One is the Nambu-Goldstone mode, which has a long wavelength, and the other is the mode with short wavelength via the EHD convection. Recently, the motion of colloidal particles dispersed in SMT has been studied, and various characteristic phenomena have been observed [18–21]. For example, the distribution of a particle's velocity becomes a Lévy distribution, which is universally found in other nonequilibrium systems such as amoebas and glasses [19].

In this study, we report the dynamics of particles in WD and FWD. Although the WD and FWD are simpler systems than SMT, studies on the particles' dynamics in EHD of NLC are limited [22–24]. The athermal motion driven by the convection flow and its fluctuation are discussed using a simple stochastic model, and the origin of the enhancement in the diffusion of particles is discussed quantitatively.

II. EXPERIMENT

We used the ternary mixture of a nematic liquid crystal with negative dielectric anisotropy, *p*-methoxybenzilidene *p*-(*n*-butyl)aniline (MBBA), 0.01 wt% of a surfactant, tetrabuthylammonium bromide (TBAB), which increases the conductivity of the system, and silica colloidal particles (Hipresica, UNK) with a diameter of 10 μm. The size polydispersity of the particles is 2.5%. The volume fraction

*kimura@phys.kyushu-u.ac.jp

of the particles is about 2.0%. The sample was injected into a parallel plate cell whose gap is about 50 μm. The cell was composed of two glass plates coated with a thin indium tin oxide layer. These conductive layers are used as electrodes to apply the voltage across the sample. Their surfaces are also coated with polyimide film and are rubbed with velvet to attain the uniaxial alignment of MBBA. A sinusoidal ac electric field of 50 Hz generated by a function generator (33120A, HP) and amplified by a power amplifier (7058, Yokogawa) was applied to the sample cell. All experiments are performed at 25 °C ± 1 °C.

We used an inverted microscope (TE2000U, Nikon) with a 4× objective lens (Plan, Nikon). The images of the particles were captured by a monochrome CCD camera (ADT-33B, FLOVEL) at 1 frame/s for about 7200 s at the respective voltages. The center positions of the particles were determined by digital image analysis with IMAGEJ. The convection patterns are superimposed on that of the particles in the images. This makes direct tracking of the particle's position difficult. In the case of WD, one can obtain both images selectively by utilizing a single polarizer and varying its direction of polarization. When the polarizer is set parallel to the director, the convective pattern can be observed. When the polarizer is set perpendicular to the director, the convective pattern disappears, and only the images of the particles can be obtained. Since the density of the particles is large, the particles easily settle at the bottom of the cell. Therefore, the particles are forced to disperse by strong flow under a high voltage before the start of the experiment.

III. RESULTS AND DISCUSSION

At a slightly lower voltage than the onset of EHD convection V_c, although no convective pattern is observed, the particles start to move parallel to the director in a ballistic fashion. Since the roll pattern originates from the focusing and defocusing of light by the deformed alignment of liquid crystal [25], the invisible pattern suggests that the array of the convective roll has not formed yet at this voltage. The motion of the particles parallel to the director indicates that the global flow over the whole cell is formed before the appearance of small rolls. The existence of such a flow is probably due to the existence of some symmetry breaking in our cell, which will be discussed later.

As the roll pattern becomes clear, the oscillation of the particles around the roll axis is apparent. The amplitude of the oscillation differs from place to place a little bit. This is partly due to the fact that the respective particles rotate at different radial positions in the respective rolls. The frequency of the oscillation f monotonously increases with the applied voltage. In addition, the slow glide motion along the roll axis appears, and the glide velocity v_g also increases with the applied voltage.

Above a certain threshold voltage, the axis of the roll starts to fluctuate temporally, and the system enters the FWD regime. The break and recombination of the rolls have also been observed as shown in Fig. 1(b). The particles are not only confined to single roll but also jump to the neighbor rolls. This makes the trajectory of the particles two-dimensional.

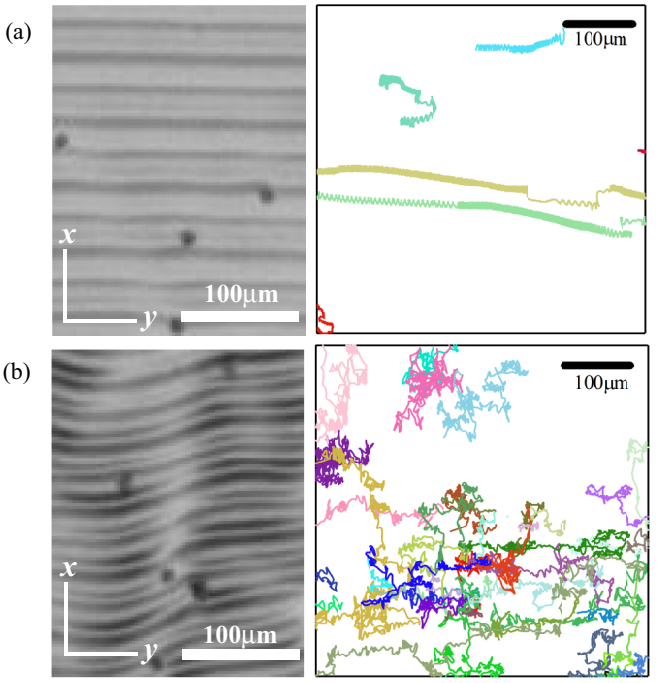

FIG. 1. (Color online) Shadowgraph image of EHD patterns and silica particles (left) and the trajectories of the dispersed silica particles (right). (a) Williams domain: stationary array of convection rolls. (b) Fluctuating Williams domain: convection rolls fluctuate their roll axis, and the defects of rolls appear.

In all voltage regions we studied, the oscillation of the particles parallel to the director has been observed. From the Fourier spectrum of the temporal change of the particle position of ten particles, we evaluate the average oscillation frequency f for the respective voltage V. The dependence of f on V is well fitted by $f \propto (V - V_c)^{0.5}$, and we obtained the critical onset voltage $V_c = 18$ V. Figure 2 shows the dependence of f on the control parameter of convection defined as $\varepsilon = (V/V_c)^2 - 1$. The best-fit curve of $f \propto \varepsilon^{0.5}$ to the experimental data is shown as a solid line in Fig. 2. In previous studies on Rayleigh-Benárd thermal convection, the convection velocity which is proportional to convection frequency is proportional to the square root of the driving energy (Rayleigh number) [26]. In SMT, the angular velocity of convection is also reported to be proportional to $\varepsilon^{0.5}$ [21].

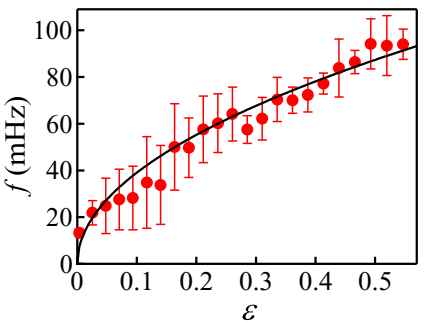

FIG. 2. (Color online) Dependence of the oscillation frequency f on the control parameter ε. The solid curve is the best fit of $\varepsilon^{0.5}$.

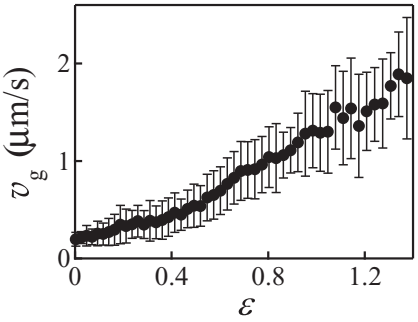

FIG. 3. Dependence of the glide velocity of the particles along the roll axis v_g on the control parameter ε. The rate of the increase of the velocity changes around $\varepsilon = 0.26$.

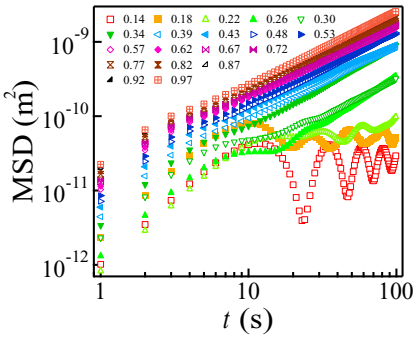

FIG. 4. (Color online) Dependence of the averaged MSD of a particle vertical to the roll axis on the elapsed time t. The different symbols are averaged data of 80 particles obtained for different ε.

However, this is different from the previous results reported for EHD with different cell geometry [22,23], where the convection velocity linearly increases with V. Although our data also can be fitted by the linear dependence of ε, the best-fit value of V_c becomes much smaller than that observed.

The particles also slowly move parallel to the axis of the roll with a constant velocity. The direction of this slow glide motion is opposite in the neighbor rolls. This indicates the helical flow exists in the respective rolls. This kind of glide motion of the particles suggests the existence of symmetry breaking in our system, which has been also discussed at $V < V_c$. Hertrich *et al.* reported a similar glide motion of particles along the roll axis in a twist nematic cell [27]. The glide velocity was reported to depend on the twist angle between the directions of the liquid crystal at the top and bottom surfaces. When the alignment is parallel, the velocity becomes zero. From the data for MBBA in Ref. [27], the estimated mismatch angle in our cell is about 6.5°. Therefore, the possible origin of the flow along the roll axis might be the mismatch of the alignment between two cell surfaces.

The glide velocity v_g monotonously increases with ε, as shown in Fig. 3. Even close to $\varepsilon = 0$, v_g exhibits a finite value. For larger ε, the rate of increase in v_g becomes larger than that for smaller ε. There is a deflection point at around $\varepsilon = 0.26$.

With an increase of the applied voltage, the pattern changes from static Williams domain [Fig. 1(a)] to dynamic fluctuating Williams domain [Fig. 1(b)]. In the FWD state, the parallel roll temporally fluctuates in the vertical direction. The oscillation of the direction of the roll axis accelerates continuously with the increase of the applied voltage (data not shown here). The threshold voltage to FWD from the change of the pattern is about $\varepsilon = 0.22$ and shows good agreement with the onset of the enhancement of v_g in Fig. 3.

In the FWD region, a particle starts to travel for a longer distance perpendicular to the roll axis. This motion relates the fluctuation of the roll axis, and the particles occasionally hop (or are pushed out) to the neighbor rolls. The creation and annihilation of defects have been reported in the FWD [28]. The fluctuation of the roll axis induces defects, and the annihilation of defects along the direction perpendicular to the roll axis creates a path connecting neighboring rolls. This enables the particles to move around many rolls. Therefore, the trajectories of the particles extend over two dimensions, as shown in Fig. 1(b).

The motion of the particles perpendicular to the roll axis is analyzed by the dependence of the MSD in this direction on the time elapsed t, as shown in Fig. 4. Below the threshold voltage of the FWD, the particles are trapped in a single roll, and MSD only oscillates with time ($\varepsilon < 0.2$). Above the onset voltage of FWD, the oscillation becomes less obvious, and the diffusion in the vertical direction becomes significant. At the short time period, the particle exhibits the oscillatory motion with a constant angular velocity Ω. Since the MSD is approximately proportional to $\sin^2(2\Omega t)$, MSD for small t is expected to be proportional to t^2. The short time temporal change of MSD obtained is proportional to $t^{1.6}$ and becomes superdiffusive or subballistic. At long time periods, the MSD becomes a linear function of t, and the motion of the particles approaches normal diffusion. We can evaluate the effective diffusion constant D from data at large t as $D = \lim_{t\to\infty} \mathrm{MSD}/(2t)$.

The dependence of the effective diffusion constant D on ε is shown in Fig. 5. The dependence can be well fitted by $D \propto (\varepsilon - 0.22)^{0.75}$ (solid line in Fig. 5). The value of D is much larger than the molecular diffusion constant $D_m = 1.81 \times 10^{-3}$ μm^2/s, which is estimated by the Stokes-Einstein relation $D_m = k_B T/6\pi\eta a$, where k_B is the Boltzmann constant, $a = 5$ μm, $T = 298$ K, and $\eta = 0.024$ Pa s [29]. The enhancement of D is over 10^3.

The motion of the particles perpendicular to the roll axis can be simply modeled by the combination of two motions: The particles oscillate in sinusoidal fashion in a roll and hop to the neighbor roll with the probability p every half time period

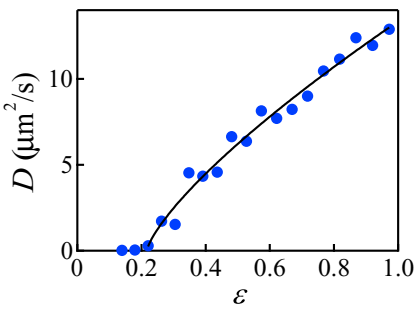

FIG. 5. (Color online) Dependence of the effective diffusion constant D on the control parameter ε. The solid curve is the best fit of $(\varepsilon - 0.22)^{0.75}$ to the data.

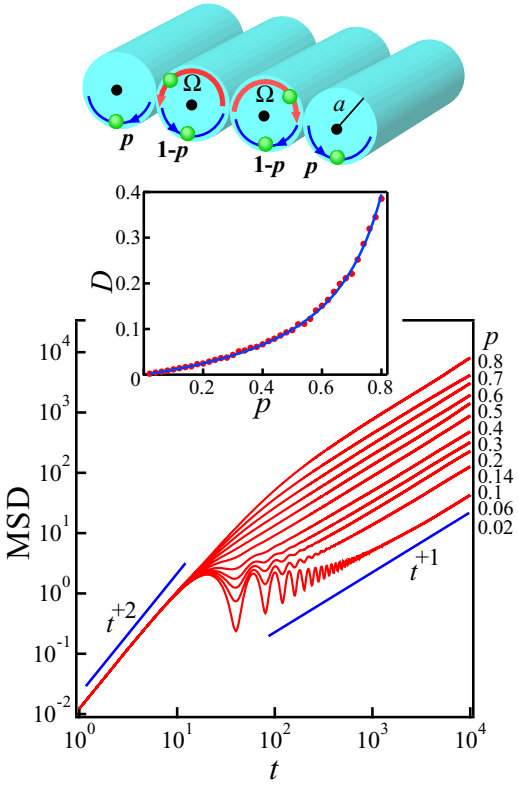

FIG. 6. (Color online) Dependence of the simulated MSD on the elapsed time t by varying the transition probability p. The respective curves are averaged for 50 samples. The upper schematic explains the situation of our simulation: A particle rotates in a roll with a constant angular velocity Ω. The particle hops to the neighbor roll with the transition probability p and remains with the same roll with probability $1-p$. The time period of the rotation is fixed to $T = 2\pi/\Omega = 40$, and the radius of a roll a is set to 1. The inset graph shows the dependence of the effective diffusion constant D on p. The best-fit curve in the inset is $D = Cp/(1-p)$ (C is constant).

of the oscillation. The particles continue to oscillate within the same roll with the probability $1-p$. The direction of the rotation in the neighbor roll is the opposite (see the schematic in Fig. 6). We simulate the motion of one particle by varying the transition probability p and calculate the averaged MDS over 50 samples starting from the various initial angular positions as shown in Fig. 6. The period of the oscillation in a roll is fixed to $T = 40$, and the radius of the roll is set to $a = 1$ in our simulation.

At the short time period, MSD is approximately proportional to t^2. This is due to the oscillatory motion at short time as already discussed. At the long time period, MSD exhibits linear time dependence. The effective diffusion constant D monotonously increases with p, as shown in the inset of Fig. 6.

To compare the simulation data with the experimental data, the both data sets are drawn in reduced scale in Fig. 7. The time is scaled by the time period of rotation $1/f$, and the MSD is scaled by D/f. The MSDs in the FWD region seem to collapse into a single master curve. The master curve looks similar to the simulated one for $p = 0.3$, as shown by the solid line in Fig. 7. The agreement between whole curves is quantitatively good. However, the slopes of the experimental curves at the short

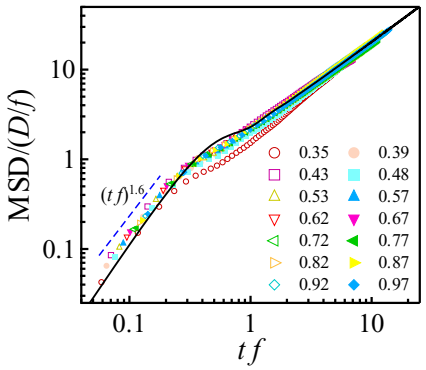

FIG. 7. (Color online) Temporal change of MSD obtained experimentally in the reduced unit for the various control parameters ε. The MSD is plotted in units of D/f. The time t is plotted in units of $1/f$. The solid line is simulated for $p = 0.3$.

time are smaller, and the experimental curves at the crossover time become dull in comparison with the simulated one. These differences are partly due to the distribution of experimental data and the influence of the fluctuation of the roll axis in FWD.

Recently, the stochastic model mentioned above has also been studied theoretically by Suzuki *et al*. [21] to discuss the diffusion of particles in the fast mode in SMT. The analytical form for the long-time diffusion constant D is obtained as $D = fd^2p/(1-p)$, where f is the frequency of the convection of the roll, d is the diameter of the roll, and p is the transition probability to the neighbor roll. The dependence of D on p is also checked by the result of our simulation as shown in the inset of Fig. 6. We apply this relation to our experimental data for the estimation of p. The frequency f is estimated from the best-fit curve in Fig. 2. We used the experimental averaged width of the oscillation $d = 16$ μm and fixed it for all ε. This value of d is much smaller than the width of the convection roll, $\approx$27 μm, as assumed in the theory. A similar small value of d has been reported in SMT [21]. From the measured D, the transition probability p is evaluated as a function of ε, as shown in Fig. 8. The value of p greatly increases with ε at the onset voltage of FWD and saturates around $p = 0.3$ for large ε. The slight variation of the experimental curves in Fig. 7 is due to the difference in p for respective ε.

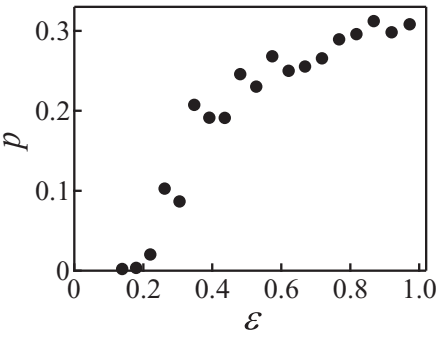

FIG. 8. Dependence of the evaluated transition probability p on the control parameter ε. The value of p rapidly increases at the onset ε from WD to FWD.

The observed enhanced diffusion constant due to EHD convection can be explained as follows: The particles are carried by the convective flow with the constant rotational velocity within a single roll. They hop to the neighbor roll stochastically due to the fluctuation of the roll axis. The enhancement of diffusion is mainly due to the increase of the velocity of convection and the increase of the hopping rate. If p does not depend on ε, D is proportional to f and is scaled as $\varepsilon^{0.5}$. This dependence of D on the control parameter is similar to that predicted for Rayleigh-Benárd convection [11,12]. The onset of vertical diffusion is due to the fluctuation of WD.

IV. CONCLUSIONS

We have studied the motion of micrometer-sized colloidal particles in the electrohydrodynamic convection of nematic liquid crystals. At the voltage region of the Williams domain, the particles exhibit a rotation around the roll axis and a glide motion along the roll axis. Above the onset voltage of the fluctuating Williams domain, the particles occasionally hop to the neighbor rolls, assisted by the fluctuation of the rolls. This varies the particles' trajectory from one-dimensional to two-dimensional. The motion perpendicular to the roll axis exhibits Brownian motion (convective diffusion) at the long time period. Its effective diffusion constant is 10^3 times larger than the molecular diffusion constant. This large enhancement lies in the difference in the mechanism of particle motion. From the simple simulation and theoretical analysis, the observed enhanced diffusion constant is quantitatively understood by a combination of the rotational motion due to the convective flow and the frequent hopping to the neighbor roll. We confirmed that the mechanism proposed for the fast mode in soft mode turbulence is also applicable to the transport of the particles in the conventional WD and FWD.

ACKNOWLEDGMENTS

The authors thank Professor T. Nagaya for the enlightening discussion on the glide motion and giving us the information on [27]. This work was supported by Grant-in-Aid for Scientific Research KAKENHI No. 23340123 from JSPS and by Innovative Areas "Fluctuation & Structure" (Grant No. 25610125) from MEXT, Japan.

[1] P. M. Chaikin and T. C. Lubensky, *Principles of Condensed Matter Physics* (Cambridge University Press, Cambridge, 1995).
[2] X. L. Wu and A. Libchaber, Phys. Rev. Lett. **84**, 3017 (2000).
[3] G. Grégoire, H. Chaté, and Y. Tu, Phys. Rev. E **64**, 011902 (2001).
[4] C. Valeriani, M. Li, J. Novosel, J. Arlt, and D. Marenduzzo, Soft Matter **7**, 5228 (2011).
[5] B. Eckhardt and S. Zammert, Eur. Phys. J. E **35**, 96 (2012).
[6] T. Toyota, D. A. Head, C. F. Schmidt, and D. Mizuno, Soft Matter **7**, 3234 (2011).
[7] See, for example, A. S. Monin and A. M. Yaglom, *Statistical Fluid Mechanics: Mechanics of Turbulence* (MIT Press, Cambridge, MA, 1975), Vol. 1.
[8] W. Y. Tam and H. L. Swinney, Phys. Rev. A **36**, 1374 (1987).
[9] T. H. Solomon and J. P. Gollub, Phys. Rev. A **38**, 6280 (1988).
[10] T. H. Solomon and J. P. Gollub, Phys. Fluids **31**, 1372 (1988).
[11] K. Ouchi, N. Mori, T. Horita, and H. Mori, Prog. Theor. Phys. **85**, 687 (1991).
[12] H. Sakaguchi, Phys. Rev. E **65**, 067201 (2002).
[13] S. Kai and K. Hiarakawa, Solid State Commun. **18**, 1573 (1976).
[14] R. Williams, J. Chem. Phys. **39**, 384 (1963).
[15] S. Kai and W. Zimmermann, Prog. Theor. Phys. **99**, 458 (1989).
[16] S. Kai, K. Hayashi, and Y. Hidaka, J. Phys. Chem. **100**, 19007 (1996).
[17] Y. Hidaka, K. Tamura, and S. Kai, Prog. Theor. Phys. **161**, 1 (2000).
[18] K. Tamura, Y. Yusuf, Y. Hidaka, and S. Kai, J. Phys. Soc. Jpn. **70**, 2805 (2001).
[19] K. Tamura, Y. Hidaka, Y. Yusuf, and S. Kai, Phys. A (Amsterdam, Neth.) **306**, 157 (2002).
[20] Y. Hidaka, Y. Hosokawa, N. Oikawa, K. Tamura, R. Anugraha, and S. Kai, Phys. D (Amsterdam, Neth.) **239**, 735 (2010).
[21] M. Suzuki, H. Sueto, Y. Hosokawa, N. Muramoto, T. Narumi, Y. Hidaka, and S. Kai, Phys. Rev. E **88**, 042147 (2013).
[22] S. Kai, N. Yoshitsune, and K. Hirakawa, J. Phys. Soc. Jpn. **40**, 267 (1976).
[23] H. Miike, Y. Kuriyama, Y. Itou, H. Hashimoto, and Y. Ebina, Phys. Rev. A **31**, 2756 (1985).
[24] C. Versace, V. Carbone, N. Scaramuzza, and D. Lucchetta, Nuovo Cimento Soc. Ital. Fis. D **16**, 1253 (1994).
[25] D. A. Penz, Phys. Rev. Lett. **24**, 1405 (1970).
[26] P. Berge and M. Dubois, Phys. Rev. Lett. **32**, 1041 (1974).
[27] A. Hertrich, A. P. Krekhov, and O. A. Scaldin, J. Phys. II **4**, 239 (1994).
[28] G. Goren, I. Procaccia, S. Rasenat, and V. Steinberg, Phys. Rev. Lett. **63**, 1237 (1989).
[29] H. Kneppe and F. Schneider, Mol. Cryst. Liq. Cryst. **65**, 23 (1981).